



Thermal stability of crystalline phases in MnO-doped zinc borosilicate glasses

G. J. Vander Stouw¹ · S. K. Sundaram¹

Received: 2 April 2020 / Accepted: 22 June 2020 / Published online: 1 July 2020
© Springer-Verlag GmbH Germany, part of Springer Nature 2020

Abstract

We have studied a relatively overlooked subset of the MnO-doped zinc borosilicate glass system with a goal of investigating the effects of MnO-doping on the thermal stability of crystalline phase formation in the system. A glass system of general composition $55\text{ZnO}-20\text{B}_2\text{O}_3-25\text{SiO}_2$ with added MnO dopant, which replaces Zn modifier locations with Mn, ratios of 0, 0.005, 0.01, and 0.015 MnO:ZnO were prepared, via batch melting at 1550 °C for 1.5 h. The glasses were characterized using differential scanning calorimetry (DSC), thermogravimetric analysis (TGA), X-ray diffraction (XRD), scanning electron microscopy (SEM), energy-dispersive spectrometry (EDS). Thermal analysis, followed by detailed XRD and Rietveld structural refinement, revealed the formation of zinc borate ($\text{Zn}_4\text{O}(\text{BO}_2)_6$), willemite (Zn_2SiO_4), and manganese zinc silicate ($(\text{ZnMn})\text{SiO}_4$) crystallites after heat-treatment at 875 °C for 4 h and zinc borate crystallites influenced by the borate anomaly in samples heated to ≈ 955 °C at a ramp rate of 10 °C/min and held for 4 h. Microstructure and elemental maps confirmed that the zinc borate had become an integral part of both glass and crystalline phases in the resulting glass–ceramic samples. MnO-content influenced the formation of the boron-containing glass phase via the borate anomaly.

Keywords Manganese dopant · High zinc content zinc borosilicate glass · Thermal analysis · Phase analysis

1 Introduction

Zinc borosilicate glasses are known for their thermal shock resistance, high elastic moduli, chemical durability, low level of optical absorbance, and the piezoelectric properties of ZnO [1, 2]. In recent years, there has been an increased interest and reporting of the fluorescent behavior of zinc borosilicate glasses through the formation of zincite, a rarer mineral form of ZnO, and willemite (Zn_2SiO_4) crystalline phases as ultraviolet (UV) emission centers [3–5]. These glasses need to be crystallized via heat-treatment, or other methods, and converted into a glass–ceramics to generate these phases, bringing the added benefits of strength, heat resistance, low production cost, and higher thermal shock

resistance at the cost of some optical clarity [4]. These glass–ceramics have recently been investigated for use in optical devices such as high energy detectors [3–5].

In our study, we chose the ternary $\text{ZnO}-\text{B}_2\text{O}_3-\text{SiO}_2$ system as a base system to study the effects of controlled post-processing thermal applications on the thermal stability of these glasses. In the chosen system, SiO_2 and B_2O_3 act as network formers. B_2O_3 additionally functions as a flux, lowering the melting point of the glass. Boron is generally found in the cubic crystalline zinc borate in four-fold coordination with oxygen, but transitions to three-fold coordination during melting [6]. Zinc oxide, responsible for forming non-bridging oxygens (NBOs) within the structure to induce a greater degree of crystallization, is present at the maximum solubility level in this system, ≈ 55 mol%, as one of two network modifiers, the other being the dopant MnO [4].

1.1 Background on MnO dopant

MnO-doped $\text{ZnO}-\text{B}_2\text{O}_3-\text{SiO}_2$ glass and glass–ceramic systems have been a topic of interest due to their potential and inherent ferromagnetic, electrical, and photoluminescent properties of MnO dopants [2, 6–9]. The Mn^{2+} in MnO,

✉ G. J. Vander Stouw
vanderstouw@gmail.com

S. K. Sundaram
sundaram@alfred.edu

¹ Ultrafast Materials Science and Engineering Laboratory (U-Lab), Kazuo Inamori School of Engineering, The New York State College of Ceramics, Alfred University, Alfred, NY, USA

the chosen dopant for this study, acts as a network modifier within the glass structure similar to the Zn^{2+} from ZnO with similar radii of approximately 0.6 Å. Mn^{2+} is a paramagnetic ion that will, in a lattice with Zn^{2+} ions, substitute for Zn^{2+} sites or otherwise occupy interstitial sites in the glass structure [6]. In glass systems containing MnO, Mn^{2+} and Mn^{3+} are expected to form, Mn^{4+} requiring specific conditions and systems [2]. The Mn^{3+} formation is due to oxidation during the melting, however, it has been shown that the ratio of Mn^{3+} ions to overall Mn ionic content will not exceed 0.03 in MnO-doped glass systems [2, 6]. The generation of Mn^{3+} leads to a range of colors from light pink to brown in doped zinc borosilicate glasses [6]. Mn^{2+} -doped zinc borosilicate glasses emit green luminescence, reddish-orange photoluminescence under UV light due to the willemite-like phases formed by four-fold coordinated Mn^{2+}/Zn^{2+} glass structure modifiers and yellowish/greenish photoluminescence as part of a glass–ceramics [6, 7]. A reddish prolonged phosphorescence has also been reported in these glasses, which becomes a yellowish and/or greenish phosphorescence after undergoing heat-treatment to form glass–ceramics [7].

In recent years, there have been a collection of papers published on the potential electrical and optical applications of unique compositions of the MnO-doped ZnO– B_2O_3 – SiO_2 system [2, 6–9]. While the Mn/Zn ratio has been noted in other studies, few utilized it as the primary form of composition alteration. Thus, it would be beneficial to study how this glass system behaves in relation to the Mn/Zn mol% ratio of the glass system. We present our data, observations, and interpretations on potential changes in thermal and structural properties of MnO-doped ZnO– B_2O_3 – SiO_2 system investigated via. heat-treatment at key transition temperatures of the system.

2 Materials and methods

2.1 Sample preparation

Glass samples were synthesized using high-purity ZnO, $MnCO_3$, H_3BO_3 , and SiO_2 powder precursors (Fisher Chemical, Alfa Aesar, Massachusetts, USA) in a platinum crucible. Four target glass compositions were chosen in the MnO-doped ZnO– B_2O_3 – SiO_2 system, where the Mn/Zn mol % ratio is 0, 0.005, 0.01, and 0.015 and MnO mol% of 0, 0.27, 0.55, and 0.82 respectively. To reduce the risk of phase separation experienced in preliminary trials and support sample homogeneity, the samples were processed following a consistent mass of 7 g batches of compositions as shown in Table 1. The batches were melted in a platinum crucible placed in a furnace at 1550 °C and held at temperature for 1.5 h. After melting, the samples were poured onto a graphite plate mold to reduce contamination and then transferred

Table 1 Sample compositions (mol% \pm 0.005) of (ZnO, MnO)– B_2O_3 – SiO_2 glass

Composition	ZnO	B_2O_3	SiO_2	MnO
1	55.00	20.00	25.00	0.00
2	54.85	19.95	24.93	0.27
3	54.70	19.89	24.86	0.55
4	54.55	19.84	24.80	0.82

to an annealing furnace to hold at 500 °C for 1 h, followed by cooling down to room temperature via unaided cooling.

2.2 Characterization

2.2.1 Thermal properties

Glass pieces produced were ground to obtain 20–50 mg of < 250 μ m powder in preparation for characterization using differential scanning calorimetry–thermogravimetric analysis (DSC-TGA, SDT Q600, TA Instruments, Delaware, USA) to determine glass transition and other transition temperatures of the glasses. Powder samples were heated to 1300 °C in Platinum crucibles to maintain purity and crucible integrity during the process. A reference material of alumina (A-10, Almatiss, Pennsylvania, USA) was used for thermal analysis. The samples were heated at rates of 20 °C/min and 10 °C/min and cooled with an airflow of 100 mL of air per minute.

2.2.2 Phase composition

Based on DSC-TGA data, powdered samples were heat-treated for 4 h at \approx 954 °C, at a ramp rate of 10 °C/min; and at 875 °C, at a ramp rate as close to 20 °C/min as possible given the limitations of the annealing kilns available. The annealing kilns furnace available lagged to match a 20 °C/min rate. Crystal nucleation and transitional growth events were observed at both treatment temperatures. The samples were heat-treated in a platinum crucible to avoid contamination and allow for easy recovery of the crystallized samples. The crystallized powders were then reground to maintain sample homogeneity for X-ray powder diffraction (XRD, D2 Phasor, Bruker, Massachusetts, USA). The XRD scan was performed using a 5.8° opening sensor, copper tube, and generator set to 30 kV and 10 mA, over the range of 2θ values of 10°–80° with a step size of 0.03°, and a count time of 576 s/step. The XRD patterns obtained were analyzed and fit to existing material PDFs using the program Difffrac4.3. Scanning electron microscopy (SEM, SM-7800F field emission scanning electron microscope, JEOL, Tokyo, Japan) with backscatter electron imaging was used to avoid the fluorescence caused by high-energy application to Mn-doped materials. Additionally, energy dispersive spectroscopy

(EDS, EDAX, New Jersey, USA) driven chemical point analysis was completed for imaging and spot compositional analysis using texture and elemental analytical microscopy (TEAM) software. The powdered and heat-treated samples were attached to the sample holders with carbon tape, for a consistent background element, and sputter-coated with gold to avoid charging.

2.2.3 Density by Archimedes' method

The density (ρ) of 7 g samples of MnO-doped zinc borosilicate glass, with Mn:Zn ratios 0, 0.005, 0.01, and 0.015, were found for comparison to known density values for Mn-doped zinc borosilicate glass, utilizing the Archimedes' method. Mass (m) was determined with a gram balance, sample volume (V) was determined via water displacement measurement using the equation, $\rho = m/V$.

3 Results and discussion

The MnO–ZnO–B₂O₃–SiO₂ glass samples, after annealing, formed visibly clear glasses with varying intensities of brownish pink coloration that increased with the concentration of MnO, resulting from the Mn³⁺ ions that formed via oxidation. Samples consistently showed slight opalescent striations radiating from a singular location on the surface of the samples. In correlation with the findings of Ehrhart this is understood as the formation of a thin B₂O₃ phase on portions of the sample surface [6]. Achieving opalescent B₂O₃ phase separation with a certain level of purity is difficult without utilizing sodium in a Na₂O–ZnO–B₂O₃–SiO₂ system to induce phase separation. However, other oxide dopants have been proven to induce partial crystallization or liquid–liquid phase separation. [10]. Zinc borate glasses have previously been shown to separate into an opalescent B₂O₃ phase and a clear ZnO–B₂O₃ phase utilizing the immiscibility gap that occurs when ZnO < 50% mol and the melt temperature > 982 °C [6, 10]. During sample preparation, it was found that an annealing temperature of 600–630 °C led to higher degrees of liquid–liquid phase separation, as seen in Fig. 1. XRD data showed phase separation into an opalescent borate phase and a clear zinc borosilicate phase [11]. The opalescent borate phase has been found, in similar compositions, to have stronger crystallization at the surface than in the general volume of the sample [6].

The density of MnO doped zinc borosilicate glass of Mn:Zn ratios 0, 0.005, 0.01, and 0.015 as 3.061, 2.576, 2.549, and 2.745 g/cm³ ± 0.05, respectively via the Archimedes method. The density values measured were comparable, although they were slightly lower than the values of zinc borosilicate and manganese borosilicate reported in the literature by varying degrees per source [2, 4, 6, 8, 12].

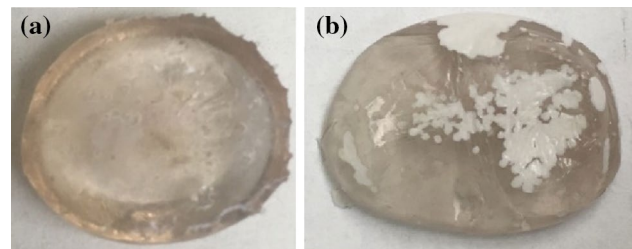


Fig. 1 (MnO, ZnO)B₂O₃–SiO glass samples with and without B₂O₃ phase separation caused by annealing at 500 °C and 620 °C (**a**, **b**)

The measured density values exhibit nonlinear decrease and increase as the Mn:Zn ratio increases, which can be attributed to the borate anomaly. MnO is similar to the alkali earth metal oxides commonly studied when examining the effects of the borate anomaly. Borate tends to form trigonal planar BO_{3/2} units in a glass matrix. Upon introduction and increase of MnO, and the electrons inherent, the borate is able to transition to tetrahedral BO_{4/2}[−] units. These units have decreased packing efficiency, decreasing the density of the material. When a key point between 0.01 and 0.015 Mn:Zn is reached the borate anomaly occurs, transitioning the borate back from BO_{4/2}[−] to BO_{3/2} units and increasing material density again [13, 14].

3.1 Thermal properties

DSC data shown in Fig. 2a and b indicated an initial endothermic transition at an onset temperature of 594–604 °C, representing the glass transition temperature (T_g) of the glass both 20 °C/min and 10 °C/min heat rates. This is notably higher T_g than that of a 40% B₂O₃ system studied by Pal et al. [15]. The endothermic valley that occurs in some compositions at T_g is an indication of the release of internal stress built into the sample [16]. Samples heat-treated at 20 °C/min exhibit decreasing T_g in samples containing MnO dopant content. The endo- and exo-thermic “start-up hooks” [16] observed in Fig. 2a indicate a difference in heat capacity between the samples and the standard material as the sample and pan weights were kept consistent. Only the sample without Mn content has an endothermic hook, suggesting a difference in heat capacity between samples with and without Mn content [16]. The temperatures of maximum crystallization (T_p) can be identified, using the exothermic nature of crystallization, as the center of exothermic peaks in the DSC curve. It must be assumed that the peaks are of similar width. The compositions under the effects of a 20 °C/min heat rate show a primary T_p of 824–826 °C. MnO-doped zinc borosilicate glass of Mn:Zn ratios 0.005, 0.01, and 0.015 produced a secondary value \approx 934 °C. This creates a point of interest in the endothermic valley between the T_p , at \approx 875 °C, where the crystallites formed by one crystal maxima

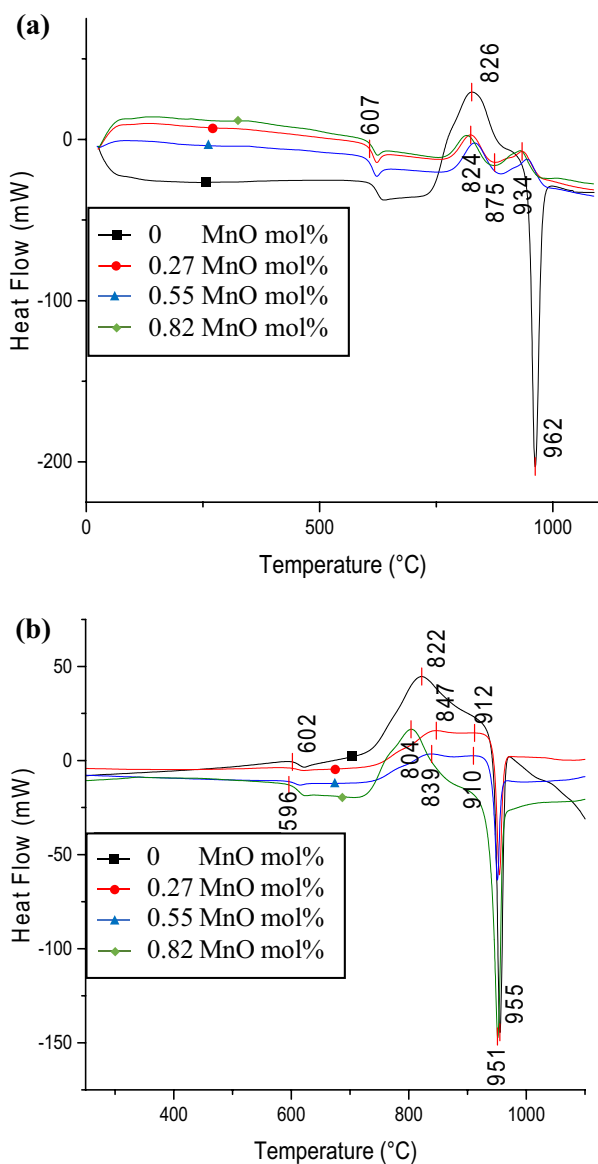


Fig. 2 DSC curves of $(\text{MnO}, \text{ZnO})\text{B}_2\text{O}_3\text{-SiO}$ glass powder, **a** at a $20\text{ }^\circ\text{C}/\text{min}$ heat rate and **b** a $10\text{ }^\circ\text{C}/\text{min}$ heat rate. T_g , T_p , and T_m temperatures are noted

have mostly subsided into the melt and the crystallites of the next crystal maxima are starting to nucleate. This point will be referred to as the crystalline transition temperature (T_{ct}). The compositions under the effects of a $10\text{ }^\circ\text{C}/\text{min}$ heating rate exhibit T_p values of $804\text{--}847\text{ }^\circ\text{C}$. It was observed that the crystallization peaks of MnO-doped zinc borosilicate glass of Mn:Zn ratios 0.005, 0.01, and 0.015 were relatively unaffected by the MnO content when heated at a $20\text{ }^\circ\text{C}/\text{min}$ heating rate. The presence of MnO in the composition was found to reduce crystallization and melting peak height in comparison to zinc borosilicate glass, which contained no MnO. When heated at a $10\text{ }^\circ\text{C}/\text{min}$ heating rate, the crystallization peaks became increasingly sharp as the MnO

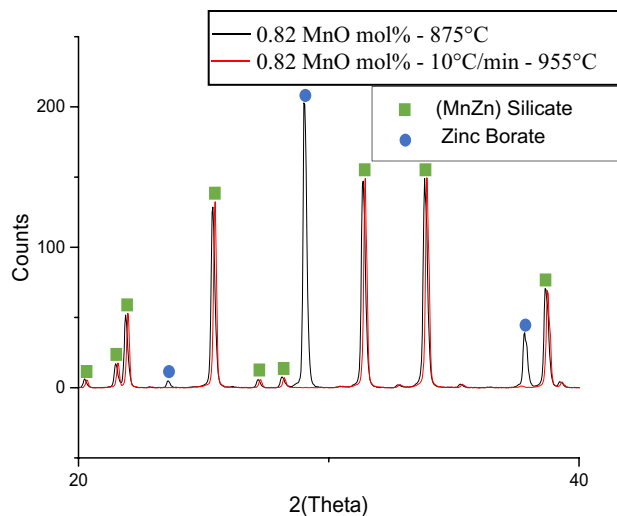


Fig. 3 XRD peaks of $(\text{MnO}_{0.015}, \text{ZnO}_1)\text{B}_2\text{O}_3\text{-SiO}$ glass powder, of Mn:Zn ratio 0.015:1 (0.82 MnO mol%), post heat-treatment to $875\text{ }^\circ\text{C}$ at $20\text{ }^\circ\text{C}/\text{min}$ and $951\text{ }^\circ\text{C}$ at $10\text{ }^\circ\text{C}/\text{min}$

content increased from MnO-doped zinc borosilicate glass of Mn:Zn ratios 0.005, 0.01, and 0.015. This is possibly due to the increasing MnO content leading to consistently forming manganese zinc silicate crystalline phase rather than glass while undergoing heat-treatment. The onset melting temperature (T_m) of the materials can be observed in the strong endothermic peak that occurs at higher temperatures. Notable peaks occur in Fig. 2b from $951\text{--}955\text{ }^\circ\text{C}$ for all compositions and in Fig. 2a at $962\text{ }^\circ\text{C}$ for zinc borosilicate glass. T_m peaks are nonexistent for MnO-doped zinc borosilicate glass at a $20\text{ }^\circ\text{C}/\text{min}$ heating rate as seen in Fig. 2a.

3.2 Phase composition

Samples of MnO-doped zinc borosilicate glass heat-treated via at the T_{ct} $875\text{ }^\circ\text{C}$ exhibited clear XRD peaks that were determined to closely match zinc borate: $\text{Zn}_4\text{O}(\text{BO}_2)_6$ (PDF 01-076-0917), willemite: Zn_2SiO_4 (PDF 04-008-0329), and manganese zinc silicate: $(\text{ZnMn})\text{SiO}_4$ (PDF 01-080-2739). Some peak shift was observed, as seen in Figs. 3 and 4. XRD analysis of a sample that had undergone heat-treatment to $\approx 954\text{ }^\circ\text{C}$ at a rate of $10\text{ }^\circ\text{C}/\text{min}$, and was subsequently mixed with high purity Si standard, was utilized to determine $\approx -0.07^\circ 2\theta$ peak shift can be attributed to instrument error as seen in Fig. 5. Samples heat-treated to $\approx 954\text{ }^\circ\text{C}$ at a rate of $10\text{ }^\circ\text{C}/\text{min}$ exhibited peak broadening in comparison to the peaks of samples raised to $875\text{ }^\circ\text{C}$ at a rate of $\approx 20\text{ }^\circ\text{C}/\text{min}$. Additionally, the zinc borate peaks observed in the former cannot be found in the later, as seen in Figs. 3 and 4b. Zinc borate and manganese zinc silicate peaks were observed with slight secondary peaks indicating willemite content, such as one near $49^\circ 2\theta$ as shown in Fig. 4a. The

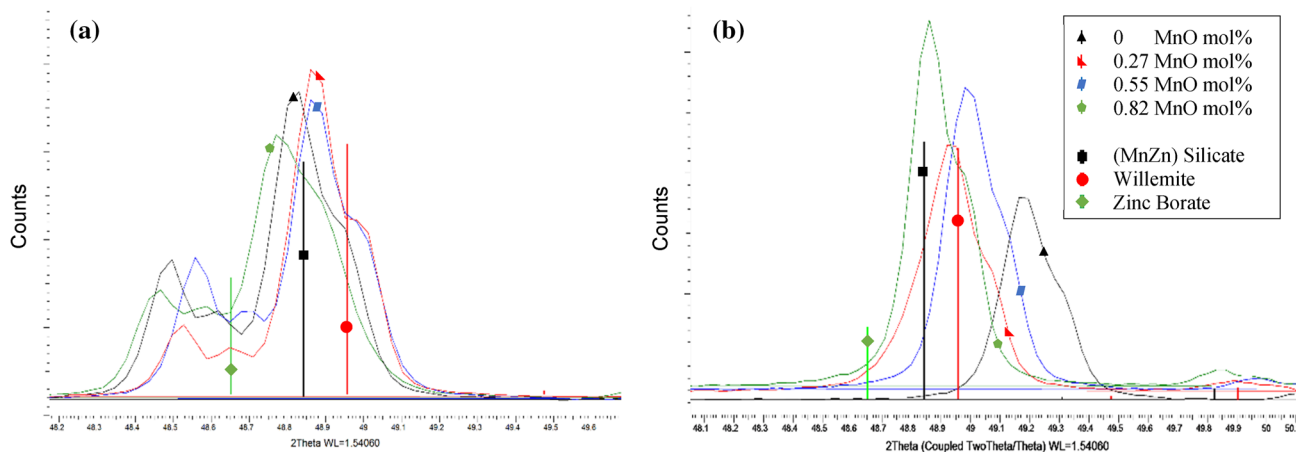


Fig. 4 XRD peaks of $(\text{MnO}_x, \text{ZnO}_1)\text{B}_2\text{O}_3\text{-SiO}$ glass powder, **a** after heat treating at 875 °C and **b** after heat treating at approximately 955 °C with a 10 °C/min heat rate, where $x=0, 0.005, 0.01, 0.015$ for compositions of MnO mol% 0–0.82 respectively

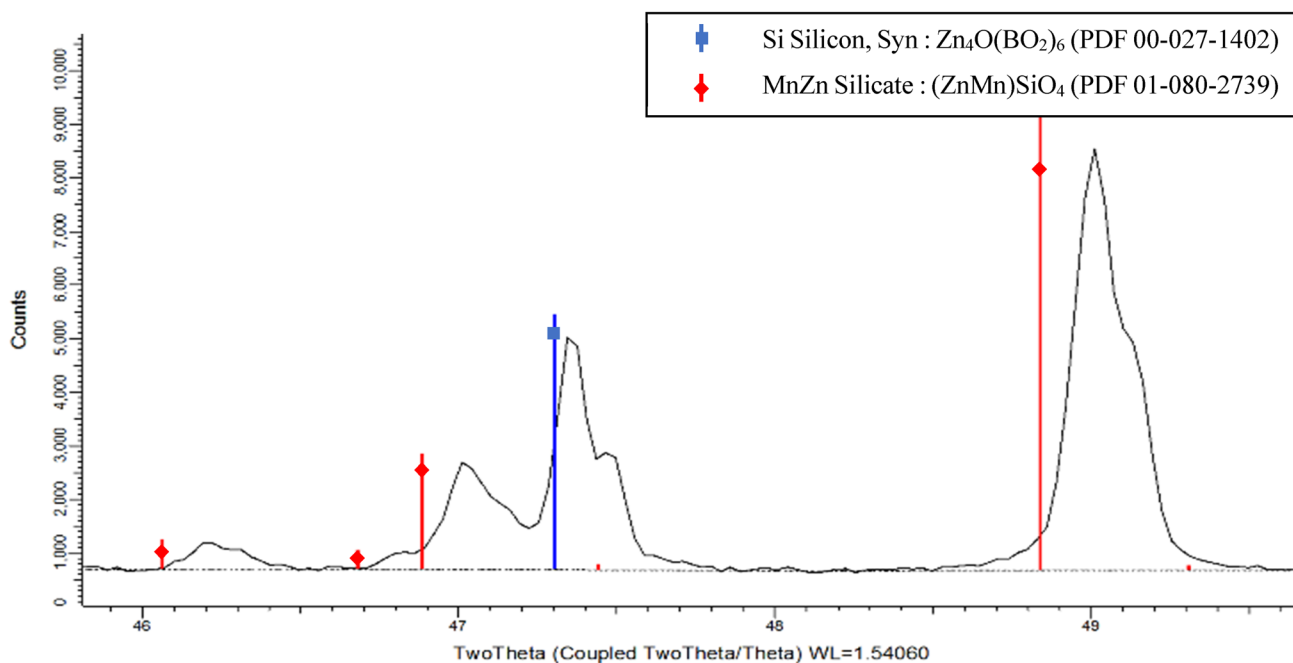


Fig. 5 XRD Peaks of $(\text{MnO}, \text{ZnO})\text{B}_2\text{O}_3\text{-SiO}$ glass powder heat treated at 951 °C via 10 °C/min ramp and mixed with high purity Si standard material to account for instrument error in peak shift

willemite secondary peaks were more pronounced in samples heat-treated to 875 °C, Fig. 4a, than those heat-treated to ≈ 954 °C, Fig. 4b. XRD peaks of samples heat-treatment to ≈ 954 °C with a 10 °C/min heating rate, exhibited a predicted peak shift away from willemite PDF 2θ values and towards manganese zinc silicate PDF 2θ values, showing a positive correlation between MnO content and manganese zinc silicate formation.

A sample of MnO-doped zinc borosilicate glass of Mn:Zn ratio 0.005 was divided into two separate particle sizes of

greater and less than 250 μm and examined for noticeable shifts in zinc borate peaks that might indicate an increase or decrease in oxygen content. The zinc borate phase has the largest atomic% of expected phases, and adsorption due to changes in the total sample surface area. The sample of particle size < 250 μm exhibited greater intensity with a small peak shift for all peaks other than $51.7^\circ 2\theta$, as seen in Fig. 6. This peak represents the only zinc borate peak in the spectra for which the peak intensity of the particle size > 250 μm is greater.

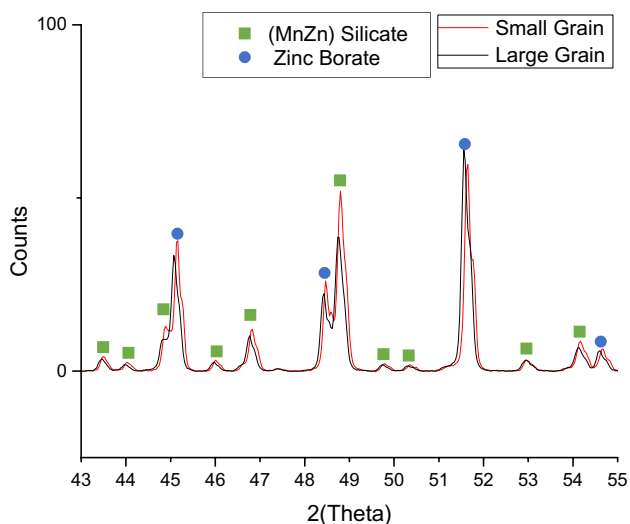


Fig. 6 Mn-doped zinc borosilicate glass powder XRD peaks for particle size comparison

It has been found that a high ZnO:B₂O₃ ratio, such as the ≈55:20 mol% ratio used in our study, can support the formation of greater volumes of willemite and lesser zinc borate [4]. The XRD peaks indicate otherwise with relatively similar peak intensity depending on 2 θ . This most likely is due to the fact the full crystallization at a T_p has not occurred. Instead, partial crystallizations have been induced by heat-treatment and cooling from the T_{ct} and T_m of the material.

Rietveld structural refinement was used to determine the approximate percentage of willemite, manganese zinc silicate, and zinc borate present in the tested samples, as reported in Tables 2, 3, 4, 5 from analysis of Figs. 7, 8, 9, 10, 11, 12, 13, 14. The (MnO,ZnO)B₂O₃-SiO₂ glass powder that underwent heat-treatment at 20 °C/min to 875 °C, the T_{ct} , showed no significant increase or decrease

in willemite, manganese zinc silicate, and zinc borate in relation to the Mn:Zn ratio post heat-treatment, maintaining approximately 35.7% zinc borate. The only exception being the MnO-doped zinc borosilicate glass powder of Mn/Zn ratio 0.005:1, which exhibited a lower 23.7% zinc borate content. The detected zinc borate content does not account for all of the B₂O₃ presents in the sample due to the tendency of borate to create amorphous trigonal planar formations in the glass matrix that are not easily detectable via XRD [17]. The chemical phase stability observed in this glass-ceramic, which has undergone heat-treatment at T_{ct} , is consistent despite the variation in Mn:Zn ratio that was applied.

Samples heat-treated to 875 °C at a heat rate of ≈ 20 °C/min exhibited a parabolic increase and decrease of both zinc borate and willemite/MnZn silicate crystallite size (Lorentzian) as MnO content is increased. No other measured factors decidedly correlate with the alterations to crystallite size. Therefore, it is unclear if a factor besides MnO content; such as the amount of glass phase formed, temperature/humidity of the room, or powder grinding technique, had any effect on the crystallite size.

Samples that underwent heat-treatment to T_m , ≈ 954 °C, at 10 °C/min indicated extremely low zinc borate content at low Mn:Zn ratios. The detectable zinc borate content peaked at ≈ 63% for 0.01 Mn:Zn before decreasing again to ≈ 38% for 0.015 Mn:Zn. The trigonal planar BO_{3/2} glass matrix structures are difficult to detect via XRD while the temporary tetrahedral BO_{4/2}⁻ crystalline structures are easily detectable. This matches the non-linear behavior of the borate anomaly previously discussed in Sect. 3 [13]. Combined with the previously discussed density findings this supports MnO, despite not being an alkali or earth alkali oxide, as having an active role in the borate anomaly within this glass composition.

Table 2 Rietveld structural refinement for post-heat-treatment zinc borosilicate glass powder XRD peaks

	Phase 1 (Inserted at temp. held at 875 °C)	Phase 2	Phase 1 (Rate: 10 °C/min, held at 955 °C)	Phase 2
Predicted phase content	Zinc borate	Willemite	Zinc borate	Willemite
Quantitative analysis—Rietveld	35.559%	64.441%	0.070%	99.930%
Space Group	I-43m	R-3	I-43m	R-3
Bragg R Value	4.039	14.444	13.305	16.996
Cry. size Lorentzian (nm)	232.0	183.1	9997.7	123.2
Crystal linear absorption coefficient (1/cm)	140.609	193.639	178.627	193.880
Crystal Density (g/cm ³)	4.238	4.262	5.384	4.267
Lattice parameters				
a (Å)	7.4814(13)	13.9311(46)	6.9077(93)	13.9239(7)
c (Å)		9.2990(07)		9.2970(51)

Analyzed in comparison to Zn₄O(BO₂)₆ (PDF 01-076-0917) and willemite: Zn₂SiO₄ (PDF 04-008-0329) phases

Table 3 Rietveld structural refinement for post-heat-treatment MnO doped zinc borosilicate glass powder, of Mn/Zn ratio 0.005:1, XRD peaks

	Phase 1 (Inserted at temp. held at 875 °C)	Phase 2 (Inserted at temp. held at 875 °C)	Phase 1 (Rate: 10 °C/min, held at 955 °C)	Phase 2 (Rate: 10 °C/min, held at 955 °C)
Predicted phase content	Zinc borate	Manganese zinc silicate	Zinc borate	Manganese zinc silicate
Quantitative analysis—Rietveld	23.682%	76.318%	2.551%	97.449%
Space group	I-43m	R-3	I-43m	R-3
Bragg <i>R</i> Value	7.774	6.614	2.845	3.115
Cry. size Lorentzian (nm)	269.2	209.9	4.2	98.2
Crystal linear absorption coefficient (1/cm)	140.666	201.826	137.168	201.327
Crystal density (g/cm ³)	4.240	4.262	4.135	4.251
Lattice parameters				
<i>a</i> (Å)	7.4804	13.9305(5)	7.5434(55)	13.9356(82)
<i>c</i> (Å)		9.2899(61)		9.3061(48)

Analyzed in comparison to Zn₄O(BO₂)₆ (PDF 01-076-0917), and manganese zinc silicate: (ZnMn)SiO₄ (PDF 01-080-2739) phases

Table 4 Rietveld structural refinement for post-heat-treatment MnO doped zinc borosilicate glass powder, of Mn/Zn ratio 0.01:1, XRD peaks

	Phase 1 (Inserted at temp. held at 875 °C)	Phase 2 (Inserted at temp. held at 875 °C)	Phase 1 (Rate: 10 °C/min, held at 955 °C)	Phase 2 (Rate: 10 °C/min, held at 955 °C)
Predicted phase content	Zinc borate	Manganese zinc silicate	Zinc borate	Manganese zinc silicate
Quantitative analysis—Rietveld	36.634%	63.366%	63.206%	36.794%
Space group	I-43m	R-3	I-43m	R-3
Bragg <i>R</i> value	3.624	4.927	1.594	3.460
Cry. size Lorentzian (nm)	241.3	190.6	0.5	141.0
Crystal linear absorption coefficient (1/cm)	140.733	201.530	193.308	201.419
Crystal density (g/cm ³)	4.242	4.255	5.827	4.253
Lattice parameters				
<i>a</i> (Å)	7.4792(11)	13.9313(68)	6.7282(97)	13.9340(18)
<i>c</i> (Å)		9.3024(95)		9.3040(79)

Analyzed in comparison to Zn₄O(BO₂)₆ (PDF 01-076-0917), and manganese zinc silicate: (ZnMn)SiO₄ (PDF 01-080-2739) phases

Table 5 Rietveld structural refinement for post-heat-treatment MnO doped zinc borosilicate glass powder, of Mn/Zn ratio 0.015:1, XRD peaks

	Phase 1 (Inserted at temp. held at 875 °C)	Phase 2 (Inserted at temp. held at 875 °C)	Phase 1 (Rate: 10 °C/min, held at 955 °C)	Phase 2 (Rate: 10 °C/min, held at 955 °C)
Predicted phase content	Zinc borate	Manganese zinc Silicate	Zinc borate	Manganese zinc silicate
Quantitative analysis—Rietveld	34.849%	65.151%	38.735%	61.265%
Space group	I-43m	R-3	I-43m	R-3
Bragg <i>R</i> value	3.518	2.694	0.327	1.830
Cry. size Lorentzian (nm)	145.8	112.9	0.6	165.2
Crystal linear absorption coefficient (1/cm)	140.512	201.282	192.924	201.302
Crystal density (g/cm ³)	4.236	4.250	5.815	4.251
Lattice parameters				
<i>a</i> (Å)	7.4831449	13.9371(38)	6.7327(57)	13.9365(45)
<i>c</i> (Å)		9.3062(57)		9.3061(21)

Analyzed in comparison to Zn₄O(BO₂)₆ (PDF 01-076-0917), and manganese zinc silicate: (ZnMn)SiO₄ (PDF 01-080-2739) phases

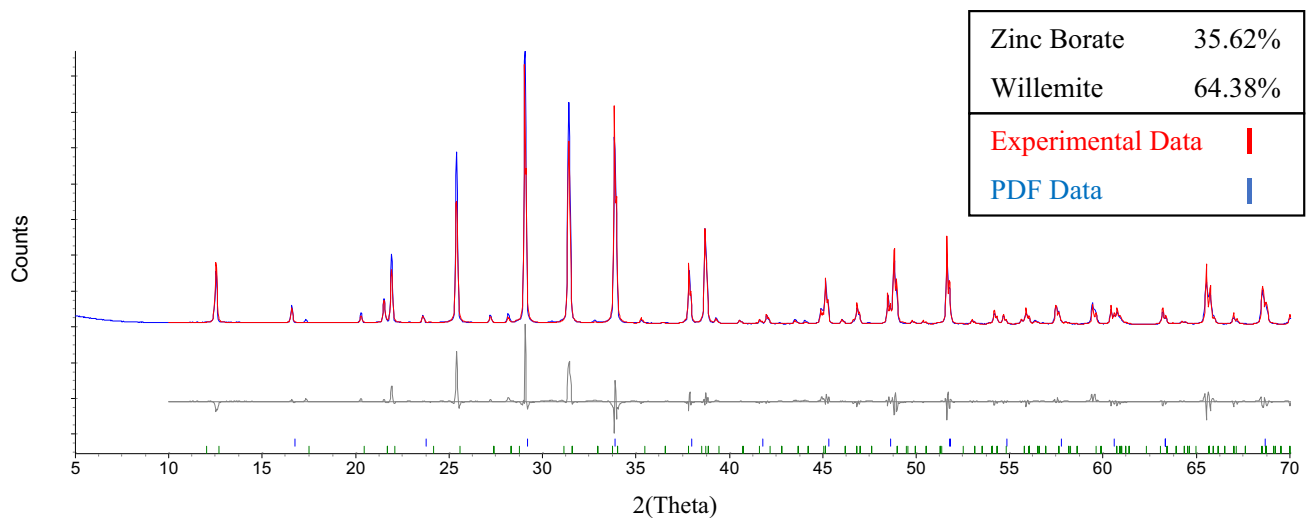


Fig. 7 Rietveld structural refinement for post heat-treatment, held at 875 °C, $(\text{MnO}_0, \text{ZnO}_1)\text{B}_2\text{O}_3\text{-SiO}$ glass powder XRD peaks. Analyzed in comparison to $\text{Zn}_4\text{O}(\text{BO}_2)_6$ (PDF 01-076-0917) and willemite: Zn_2SiO_4 (PDF 04-008-329) phases

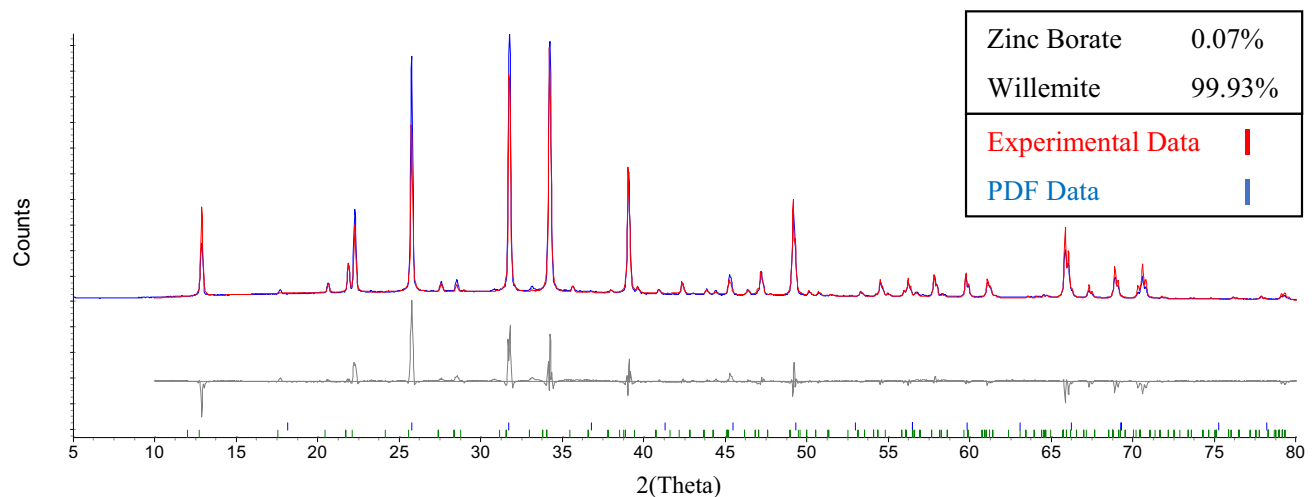


Fig. 8 Rietveld structural refinement for post-heat-treatment, ramped to and held at 955 °C at a rate of 10 °C/min, $(\text{MnO}_0, \text{ZnO}_1)\text{B}_2\text{O}_3\text{-SiO}$ glass powder XRD peaks. Analyzed in comparison to $\text{Zn}_4\text{O}(\text{BO}_2)_6$ (PDF 01-076-0917) and willemite: Zn_2SiO_4 (PDF 04-008-329) phases

The crystal size Lorentzian of the zinc borate phase post heat-treatment to ≈ 954 °C at a rate of 10 °C/min was measured to be between 0.5–4.2 nm in glass compositions containing MnO, a notable difference from the ≈ 150 –250 nm exhibited by the same compositions following heat-treatment to 875 °C at a rate of ≈ 20 °C/min. The crystal size Lorentzian measured for the ≈ 954 °C heat-treatment is so small that it calls into question whether crystallites are even forming in the T_m based heat-treatment, or whether the detected “crystallites” are instead protocrystals. This suggests that heat treatment at the T_m rather than at the T_{ct} induces a situation where an amorphous glass phase is allowed to form

dispersed protocrystals directly prior to cooling into its crystal matrix and could be grounds for further study.

SEM spot analysis and EDS chemical mapping were used to further analyze the surface of selected crystallites for the expected chemical composition found via XRD and Rietveld structural refinement, as shown in Figs. 15a–e. The findings of the EDS chemical mapping were in relatively close agreement with the Rietveld data, with exception to the inability of this surface analysis technique to properly identifying boron content. In Fig. 15a, for example, the B and Mn content of the zinc borosilicate glass were measured at 2%. This indicated both an inability to properly detect boron, as the

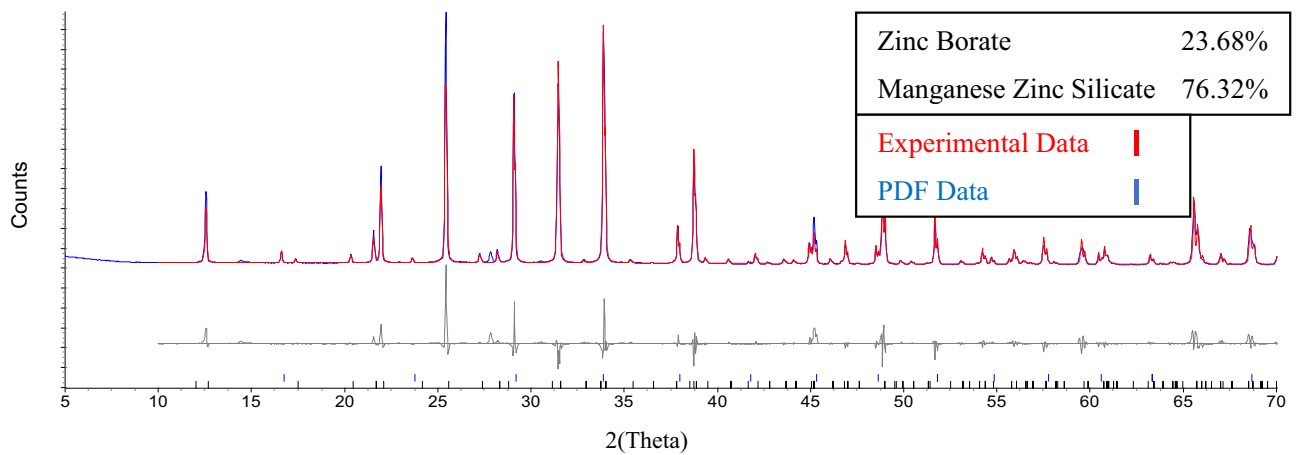


Fig. 9 Rietveld structural refinement for post-heat-treatment, held at 875 °C, $(\text{MnO}_{0.005}, \text{ZnO}_1)\text{B}_2\text{O}_3\text{-SiO}$ glass powder XRD peaks. Analyzed in comparison to $\text{Zn}_4\text{O}(\text{BO}_2)_6$ (PDF 01-076-0917) and willemite: Zn_2SiO_4 (PDF 04-008-0329) phases

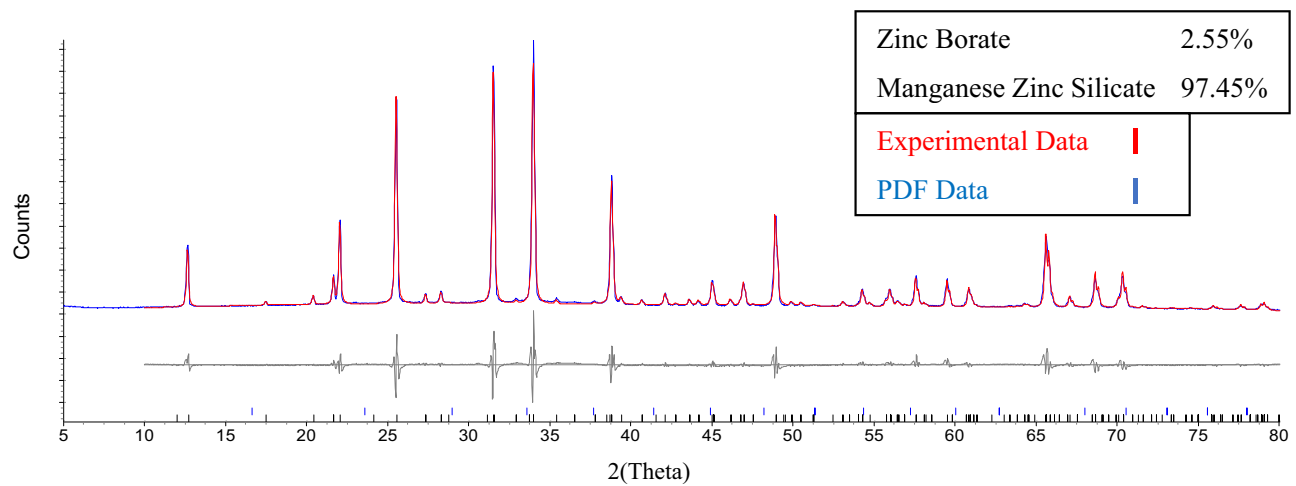


Fig. 10 Rietveld structural refinement for post-heat-treatment, ramped to and held at 955 °C at a rate of 10 °C/min, $(\text{MnO}_{0.005}, \text{ZnO}_1)\text{B}_2\text{O}_3\text{-SiO}$ glass powder XRD peaks. Analyzed in comparison to $\text{Zn}_4\text{O}(\text{BO}_2)_6$ (PDF 01-076-0917) and willemite: Zn_2SiO_4 (PDF 04-008-0329) phases

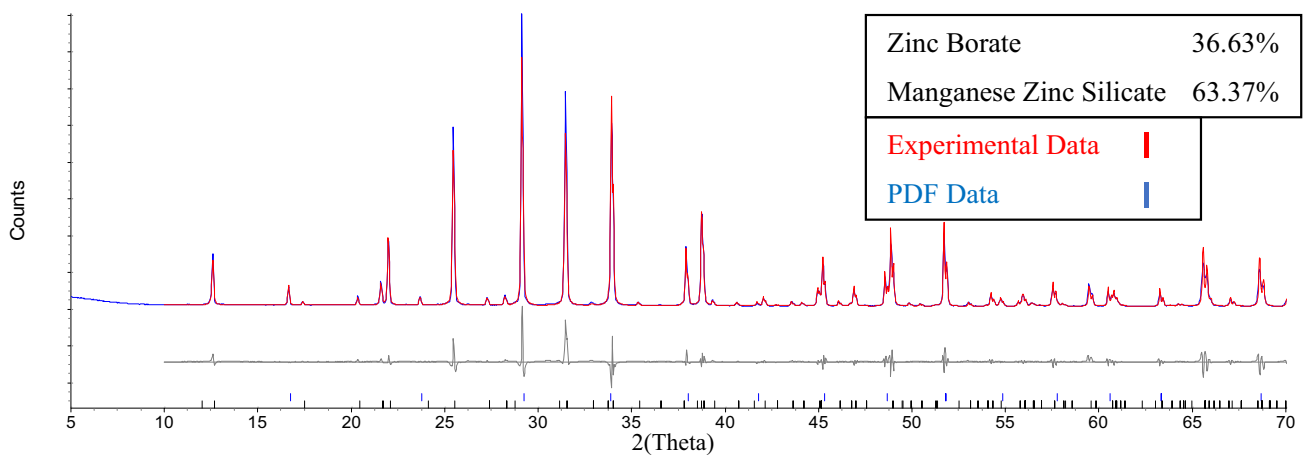


Fig. 11 Rietveld structural refinement for post-heat-treatment, held at 875 °C, $(\text{MnO}_{0.01}, \text{ZnO}_1)\text{B}_2\text{O}_3\text{-SiO}$ glass powder XRD peaks. Analyzed in comparison to $\text{Zn}_4\text{O}(\text{BO}_2)_6$ (PDF 01-076-0917) and willemite: Zn_2SiO_4 (PDF 04-008-0329) phases

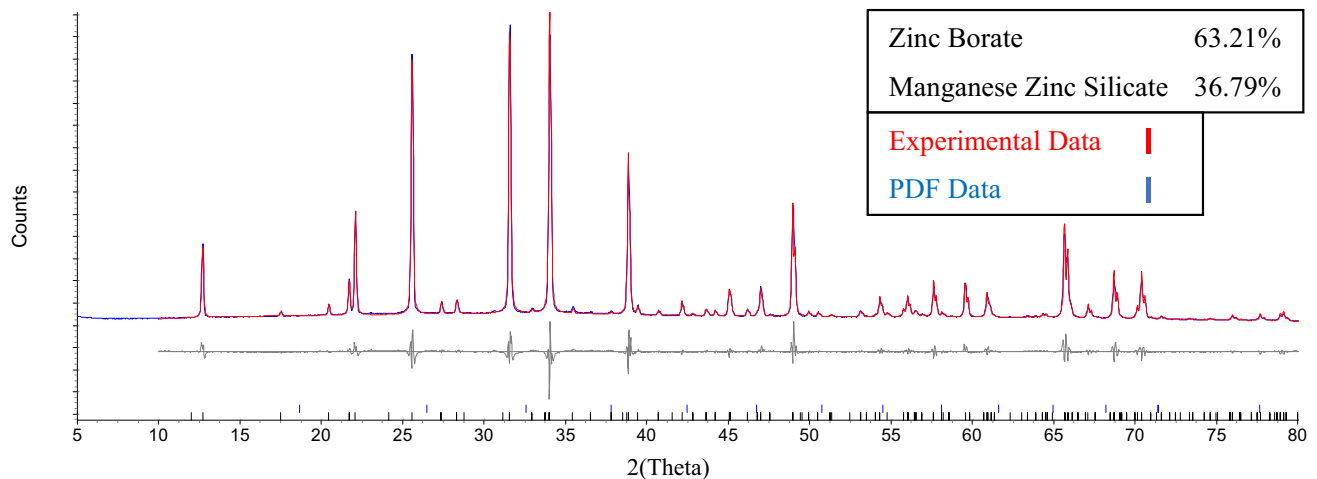


Fig. 12 Rietveld structural refinement for post-heat-treatment ramped to and held at 955 °C at a rate of 10 °C/min, $(\text{MnO}_{0.01}, \text{ZnO}_1)\text{B}_2\text{O}_3\text{-SiO}$ glass powder XRD peaks. Analyzed in comparison to $\text{Zn}_4\text{O}(\text{BO}_2)_6$ (PDF 01-076-0917) and willemite: Zn_2SiO_4 (PDF 04-008-0329) phases

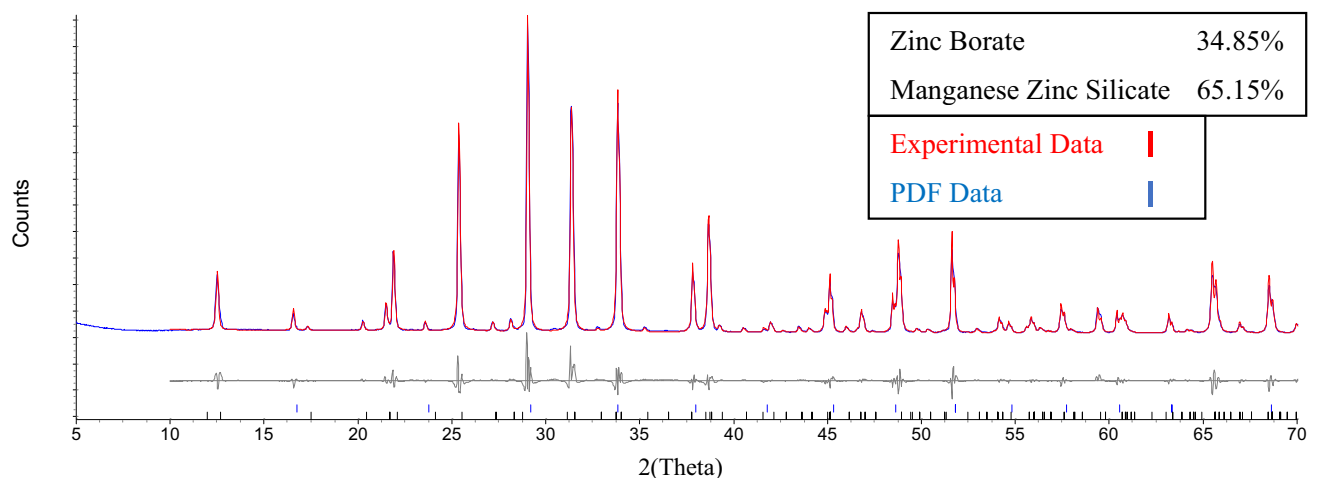


Fig. 13 Rietveld structural refinement for post-heat-treatment, held at 875 °C, $(\text{MnO}_{0.015}, \text{ZnO}_1)\text{B}_2\text{O}_3\text{-SiO}$ glass powder XRD peaks. Analyzed in comparison to $\text{Zn}_4\text{O}(\text{BO}_2)_6$ (PDF 01-076-0917) and willemite: Zn_2SiO_4 (PDF 04-008-0329) phases

composition has 20 mol % B_2O_3 , and a case of false positive, as zinc borosilicate glass contains no Mn.

Based on the O and Zn contents, the crystallites observed in Fig. 15a are attributed to zinc borate formation, which has hexagonal structures, with surface boron oxidation. Although willemite is also known to form trigonal hexagonal crystal systems [18], there was minimal silicon detected at these locations in comparison to zinc and oxygen content. There were also areas that exhibited a mixture of zinc and silica, where the expected zinc silicate, willemite, would form.

Chemical mapping and EDS imaging of MnO doped zinc borosilicate glass of Mn:Zn ratio 0.005 revealed three structural features of interest; the first of which is the lighter colored formations, fractured from the grinding process,

of zinc borate as can be seen by the O and Zn contents in Fig. 15b. Mn content can only be observed in locations where Zn can be directly observed due to Mn replacing Zn locations in the matrix. This supports that Mn is replacing zinc in both willemite and zinc borate structures.

The second structural feature of interest is the porous formation that appears in some sections of zinc borate, seen in Fig. 15b, c. These pores are potentially pockets leftover from locations where material was decomposing out of the melt but became trapped via the cooling process. While excessive bubbling was not observed in the glass samples during sample preparation, micron scale bubbles may have gone unnoticed.

The third structural feature appeared to be either a glassy SiO_2 phase or a crystalline manganese zinc

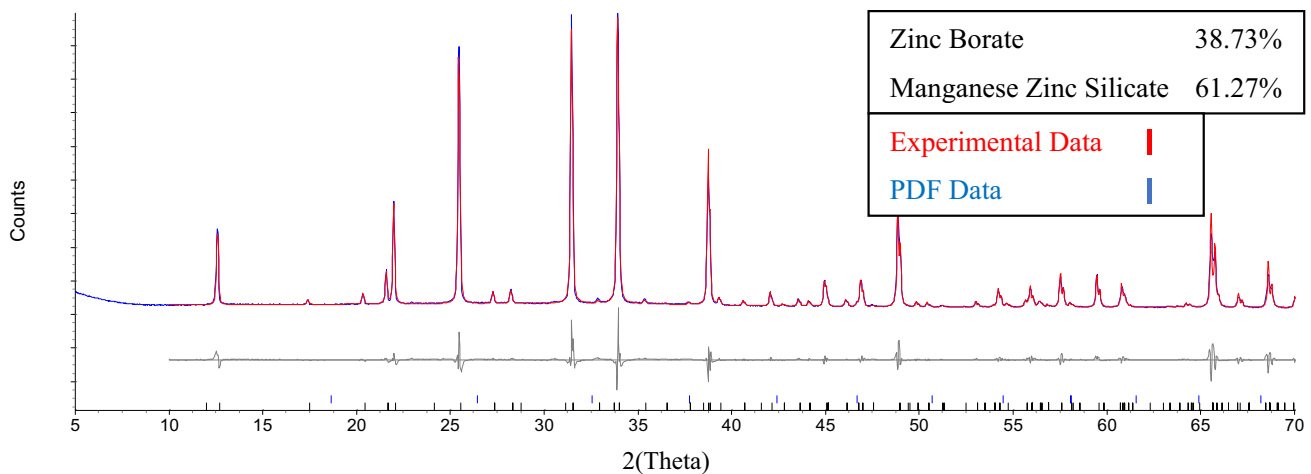


Fig. 14 Rietveld structural refinement for post-heat-treatment, ramped to and held at 955 °C at a rate of 10 °C/min, $(\text{MnO}_{0.015}, \text{ZnO})\text{B}_2\text{O}_3\text{-SiO}_2$ glass powder XRD peaks. Analyzed in comparison to $\text{Zn}_4\text{O}(\text{BO}_2)_6$ (PDF 01-076-0917) and willemite: Zn_2SiO_4 (PDF 04-008-0329) phases

silicate phase due to detecting primarily silica, as seen in Fig. 15b–d. The lack of consistent indication of Zn, Mn, or B suggests that this is a glass phase and that the zinc borate and willemite/Mn Zn silicate phases detected via XRD may be the two lighter colored phases observed in Fig. 15e.

A sample of MnO-doped zinc borosilicate glass of Mn:Zn ratio 0.015, under heat-treatment to 875 °C at a rate of ≈ 20 °C/min, exhibited a structure primarily formed of Zn that appeared hexagonal in sections with raised boundaries (like walls) made of a mixture of O and Zn, as seen in Fig. 15d. Similar to the structures observed in Fig. 15a, and those studied by Self et al., these formations are understood to be a form of fractured zinc oxide microdisks [19, 20]. The deformation of the hexagonal structure is due to either modification to a zinc borate phase, or the heat-treatment at the transition point between two crystal maxima causing the crystallites to deform. The hexagonal structures formed above and next to what appeared to be either crystalline willemite, manganese zinc silicate, or glass silicate phase. Counter to the varied structures found in samples post-heat-treatment to 875 °C, at a rate of ≈ 20 °C/min, samples heat-treated to ≈ 954 °C at a rate of 10 °C/min consistently exhibited the three structural features seen in Fig. 16.

The first consisted of inclusions of SiO_2 which had broken from the surrounding phases due to a differing rate of thermal expansion, observed in yellow (Si), light green (O), and a distinct lack of dark green (Zn) in Fig. 16. The remaining two features existed as an occasionally

porous phase, mixed intermittently with a smooth phase, both containing comparable Zn content. The pores of the former were due to either small SiO_2 inclusions or prior decomposition. These phases can be differentiated via O and Si content to be willemite/(Mn,Zn)silicate and zinc borate, respectively. Neither B nor Mn could be detected sufficiently to map in any of the four glass compositions, as seen in Fig. 16.

4 Conclusions

MnO-doped zinc borosilicate glass of Mn:Zn ratios 0.005:1, 0.01:1, and 0.015:1 heat-treated at a rate of 20 °C/min were found to be relatively resistant to induced structural alteration via rapid heating rates, as DSC peaks exhibited were relatively broad and exhibited few rapid changes in heat flow. When heat-treated at the transition point between two crystalline maxima, 875 °C, samples exhibited a variety of structures as a glass–ceramics of consistent zinc borate and willemite/(Mn,Zn) silicate crystalline phase percentages, regardless of Mn:Zn ratio and no manganese borate. Samples heat-treated to the T_m , ≈ 955 °C, at a rate of 10 °C/min showed nucleation of SiO_2 inclusions and willemite/manganese zinc silicate crystallites in a zinc borosilicate glass/protocrystal matrix. The zinc borate structural state in these samples is nonlinearly influenced by the Mn:Zn ratio via the borate anomaly.

Fig. 15 EDS elemental mapping of **a** $(\text{MnO}_0, \text{ZnO}_1)\text{B}_2\text{O}_3\text{-SiO}_2$, **b-d** $(\text{MnO}_{0.005}, \text{ZnO}_1)\text{B}_2\text{O}_3\text{-SiO}_2$, and **e** $(\text{MnO}_{0.015}, \text{ZnO}_1)\text{B}_2\text{O}_3\text{-SiO}_2$ glass powder post heat-treatment at 875 °C

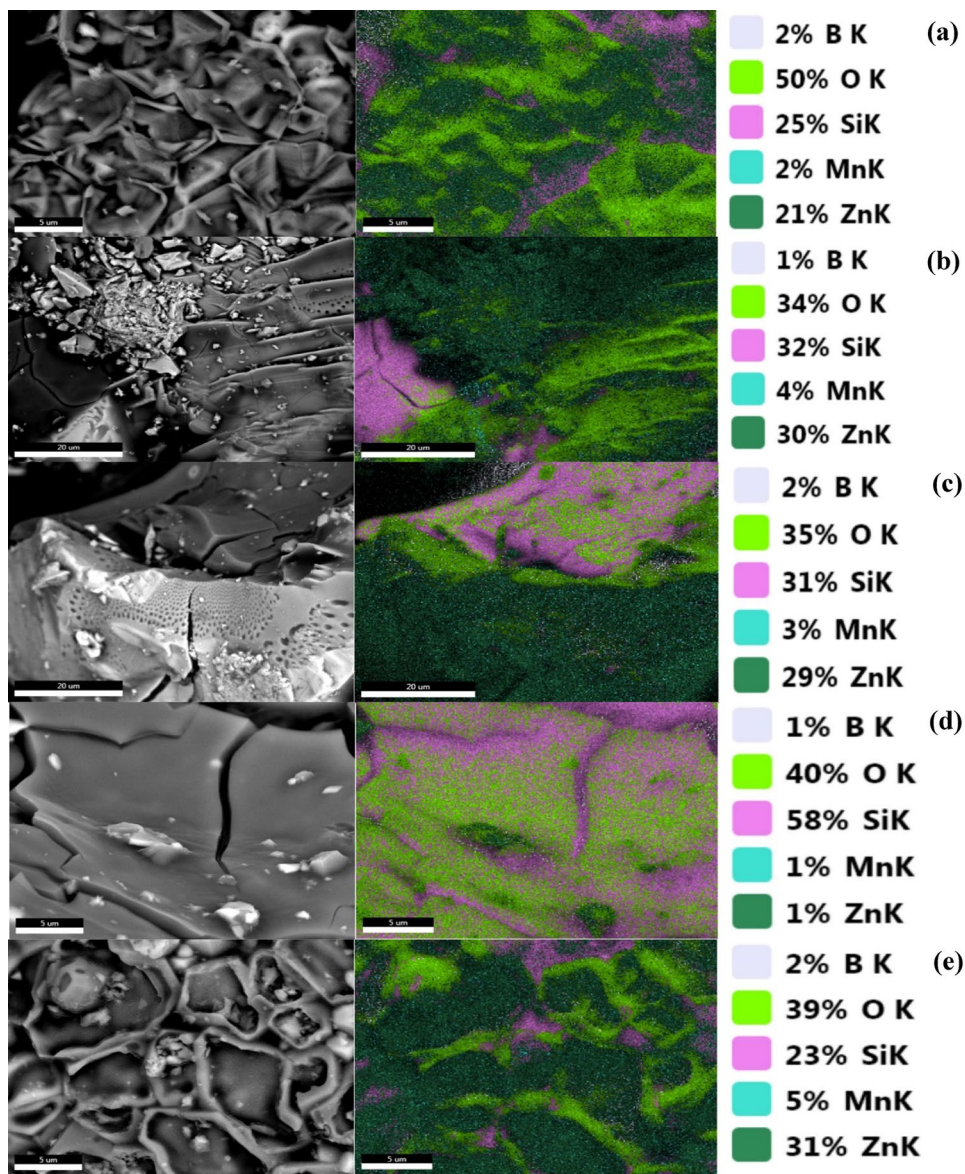
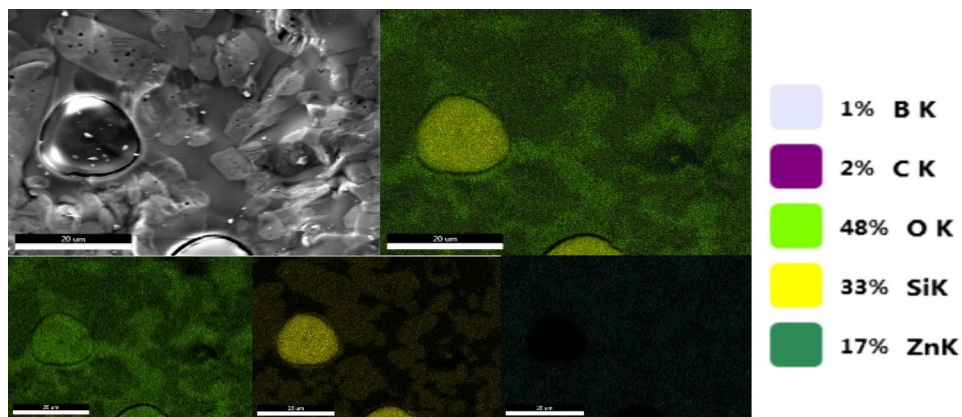


Fig. 16 EDS elemental mapping of $(\text{MnO}_0, \text{ZnO}_1)\text{B}_2\text{O}_3\text{-SiO}_2$ glass powder heat-treated to 955 °C at a rate of 10 °C/min



Acknowledgements GJVS acknowledges the support from Professors Alexis Clare, Steven Tidrow, Darren Stohr, and Scott Mixture and Graduate Student Charles Bellows. GJVU also acknowledges all the support from Inamori School of Engineering. SKS acknowledges the support from Kyocera Corporation in the form of the Inamori Professorship.

Author contributions SKS advised and supervised the project. GVS prepared samples, performed: thermal annealing, measurements, analysis, and wrote the manuscript text. SKS and GVS worked together to design and initiate testing and iteratively revise the manuscript.

Funding This project was funded by the Inamori School of Engineering at Alfred University.

Compliance with ethical standards

Conflicts of interest The authors declare no competing financial interests.

References

1. E. Hamilton, R. Waxler, J. Nivert Jr., *J. Res. Natl. Bur. Stand.* **62**, 59–62 (1959)
2. P. Kupracz, J. Karczewski, M. Przeźniak-Welenc, N.A. Szreder, M.J. Winiarski, T. Klimczuk, R.J. Barczyński, *J. Noncryst. Solids* **423–424**, 68–75 (2015)
3. G. Chen, M. Nikl, N. Solovieva, A. Beitlerova, J. Rao, Y. Yang, Y. Zhang, X. Jiang, C. Zhu, *Radiat. Meas.* **38**, 771–774 (2004)
4. A.T.G. Kullberg, A.A.S. Lopes, J.P.B. Veiga, M.M.R.A. Lima, R.C.C. Monteiro, *J. Noncryst. Solids* **441**, 79–85 (2016)
5. A.T.G. Kullberg, A.A.S. Lopes, J.P.B. Veiga, R.C.C. Monteiro, *J. Cryst. Growth* **457**, 239–243 (2017)
6. D. Ehrhart, *Glass Sci. Technol. J.* **54**, 65–75 (2013)
7. C. Li, Q. Su, S. Wang, *Mater. Res. Bull.* **37**, 1443–1449 (2002)
8. E.F. Keskenler, S. Doğan, G. Turgut, B. Gürbulak, *Metall. Mater. Trans.* **43**, 5088–5095 (2012)
9. P. Kupracz, A. Lenarciak, M. Łapiński, M. Przeźniak-Welenc, N.A. Wójcik, R.J. Barczyński, *J. Noncryst. Solids* **458**, 15–21 (2017)
10. M. Soleimaanzade, B.E. Yekta, V. Marghussian, *Int. J. Appl. Glass Sci.* **5**(2), 185–192 (2014)
11. S. Guilherme, F. Vladimir, C. Rodrigues, A.C. Rodrigues, E. Zanotto, J. Lumeau, L. Glebova, L.B. Glebova, *J. Am. Ceram. Soc.* **94**(1), 145–150 (2011)
12. K. Dixon, *N.Y.S. Coll. of Ceram. at Alfred Univ.* 1–26 (2017).
13. M. Eigen, *Elsevier Sci. Ltd Struct. Chem. Glasses* **2002**, 463–511 (2002)
14. M. Bengisu, *J. Mater. Sci.* **51**(5), 2199–2242 (2016)
15. M. Pal, B. Roy, M. Pal, *J. Mod. Phys.* **2**, 9 (2011)
16. L. Thomas, *TA Instrum.* 1–5 (2010)
17. A. Wright, *Int. J. Appl. Glass Sci.* **6**, 45–63 (2015)
18. G. Essalah, G. Kadim, A. Jabar, R. Masrouf, M. Ellouze, H. Guermazi, S. Guermazi, *Ceram. Int.* **46**(8), 12656–12664 (2020)
19. K. Self, H. Zhou, H. Greer, Z. Tian, W. Zhou, *Chem. Commun.* **49**, 5411–5413 (2013)
20. I. Kazeminezhad, R. Yousefi, *Solid State Sci.* **14**, 349–353 (2012)

Publisher's Note Springer Nature remains neutral with regard to jurisdictional claims in published maps and institutional affiliations.